J. Fluid Mech. (1973), *vol.* 60, *part* 4, *pp.* 665–687
Printed in Great Britain

Experiments on swirling turbulent flows. Part 1. Similarity in swirling flows

By K. S. YAJNIK AND M. V. SUBBAIAH
National Aeronautical Laboratory, Bangalore, India

(Received 22 September 1972 and in revised form 17 May 1973)

The effects of swirl on internal turbulent flows are studied by conducting experiments on turbulent pipe flow with variable initial swirl. This first part of the study is primarily concerned with similarity laws. The mean velocity profiles, both away from and close to the wall, are found to admit similarity representations at sufficiently large Reynolds numbers, provided that flow reversal does not take place near the entrance. While the wall law is not sensibly dependent on swirl, the velocity defect law in its extended form is sensitive to swirl. Further, a logarithmic skin-friction law is obtained in which only the additive coefficient depends on swirl. This coefficient is found to vary linearly with the swirl angle in the range of the present experiments.

1. Introduction

Several applications have intensified interest in swirling turbulent flows. The possibility of increasing the heat-transfer rate in a heat exchanger by introducing swirl without paying the penalty of excessive skin friction has motivated several investigations (for example, Kreith & Margolis 1959; Smithberg & Landis 1964; Migay & Golubev 1970). Sensitivity of duct discharge to swirl has led to the development of certain fluidic devices and to investigations of the thrust control of rocket nozzles (Mager 1971). Recent interest in optimization of high speed centrifuges has also triggered investigations (Krause & Hirschel 1970).

This paper deals with swirling turbulent flow in a stationary pipe, which is one of the simplest swirling turbulent flows and which can be controlled sufficiently well for careful experiments. Further, it could give insight into the properties of three-dimensional turbulent boundary layers.

Decay of angular momentum in a swirling pipe flow was the theme of some of the early investigations. Talbot (1954) analysed the laminar case on the assumption that the axial velocity profile was slightly distorted by swirl, and the predicted exponential decay was supported by experiments (see also Kiya, Fukusako & Arie 1971). A similar analysis was carried out for turbulent flow by Kreith & Sonju (1965), on the basis of an assumed axial mean velocity profile given by the $\frac{1}{7}$ power law with a small perturbation, and an assumed eddy viscosity for the tangential direction. The decay of angular momentum measured by a vane rotor agreed well with the predictions (see also Wolf, Lavan & Fejer 1969).

Effects of swirl on skin friction and heat transfer have also been investigated.

Author(s)	Approximate pipe diameter (mm)	Length/ diameter	*Re*	Fluid	Swirl generation	Comments
Talbot (1954)	31	45	170–2700	Water	Rotating a section of test pipe	V by motion-picture studies, stability of swirl
Binnie (1957)	50	35	60–260	Water	Rotating a section of test pipe	Flow visualization by dye injection
Koch (1958)	50	20	2×10^3–5×10^4	Air	Twisted tapes	Friction factor by pressure-drop measurements and heat-transfer measurements. $H/D = 5{\cdot}0$–$22{\cdot}0$
Kreith & Margolis (1959)	13	80	10^4–10^5	Air and water	Coiled wires and twisted tapes	Friction factor by pressure-drop measurements and heat-transfer measurements. $H/D = 5{\cdot}2$–$14{\cdot}6$
Smithberg & Landis (1964)	35	30	$0{\cdot}6 \times 10^4$–6×10^4	Air and water	Twisted tapes	Friction factor by pressure-drop measurements and heat-transfer measurements. $H/D = 3{\cdot}6$–$22{\cdot}0$
Kreith & Sonju (1965)	25	100	10^4–10^5	Water	Twisted tapes	Average swirl using swirl vane meter. $H/D = 9, 15$
Sachdeva (1968)	50	22	10^4–10^5	Water	Tangential inlets	U, V, friction factor by pressure-drop measurements. Flow visualization

Author(s)	Approximate pipe diameter (mm)	Length/ diameter	*Re*	Fluid	Swirl generation	Comments
Wolf *et al.* (1969)	75	72	$0{\cdot}8 \times 10^5$–$3{\cdot}6 \times 10^5$	Air	Entry vanes	U, V and streamwise turbulent intensity
Migay & Golubev (1970)	34	120	10^4–10^5	Air and water	Entry vanes	Friction factor by pressure-drop measurements and heat-transfer measurements
Senoo & Negata (1972)	150	60	$1{\cdot}85 \times 10^5$	Air	Entry vanes	Direction and total pressure of flow, skin friction by pressure drop, effect of roughness for swirl numbers up to 0·8
Present	120·5	100	$0{\cdot}4 \times 10^5$–$2{\cdot}6 \times 10^5$	Air	Entry vanes	U, V, skin friction, streamwise turbulence intensity spectrum of turbulence. Measurements are reported for swirl angles up to 13·5°

TABLE 1. Summary of major swirl flow experiments

For instance, Koch (1958), Kreith & Margolis (1959) and Smithberg & Landis (1964) reported skin-friction data. Parameters governing their experiments are compared with those of the present experiments in table 1.

Very few velocity measurements have been reported. In one set of experiments (Rochino & Lavan 1969; Wolf *et al.* 1969), qualitative results obtained with static and impulse probes, which were aligned in the flow direction indicated by yaw probes, showed a flat axial velocity profile and an almost linear variation of tangential velocity away from the wall.

The striking phenomenon of flow reversal attracted considerable attention. Following early observations of Nuttal (1953), Binnie & Teare (1956), Binnie (1957) and Gore & Ranz (1964) made detailed observations and confirmed the possibility of a central cylindrical region of reversed axial flow. Experiments of Sachdeva (1968) have shown that reversed flow can occur in an annular region.

Clearly, the effect of swirl on axial flow can indeed be very large and an analysis based on small perturbations in axial velocity is restricted in scope. A search for an alternative and possibly more general basis suggested similarity as a conceivable property which could be exploited both for correlating data as well as for the formulation of analysis. Hence a major concern of this paper is to study similarity properties experimentally.†

Several alternative approaches have been attempted. For instance, Lavan and his co-workers (Lavan, Nielsen & Fejer 1969) carried out an analysis based on small perturbations of solid-body rotation for small axial Reynolds numbers up to about 20. In another investigation, Rochino & Lavan (1969) analysed the flow using an empirical axial velocity profile which does not change in the streamwise direction. Modified vorticity transport theory and von Kármán's local similarity hypothesis were also employed. Discrepancies however appeared when the flow was predominantly irrotational or in solid-body rotation. Finite-difference computational schemes (for instance, Siddhartha 1971) have also been used with suitable closure hypotheses. But the reliability of such computations is seriously affected by the nature of closure hypothesis describing three-dimensional flows.

The plan of this study is to describe experiments on similarity properties in the first part and further experiments on the effect of swirl on turbulence, flow development and effects of flow reversal in the second part. The next section of this part contains a description of the experimental technique. The suitability of various swirl parameters is discussed in §3. A critical discussion of skin-friction measurement in swirling flows is given in §4. Since similarity representation can be interpreted as a state which the flow attains asymptotically at large distances from the entrance, various alternative modes are discussed in §5. The results are finally given in the last section.

† Kinney (1967) extended von Kármán's similarity hypothesis in order to establish conditions under which universal velocity similarity exists for plane rotating turbulent flow. The similarity laws which are investigated in this paper are distinct from the closure hypothesis considered by Kinney.

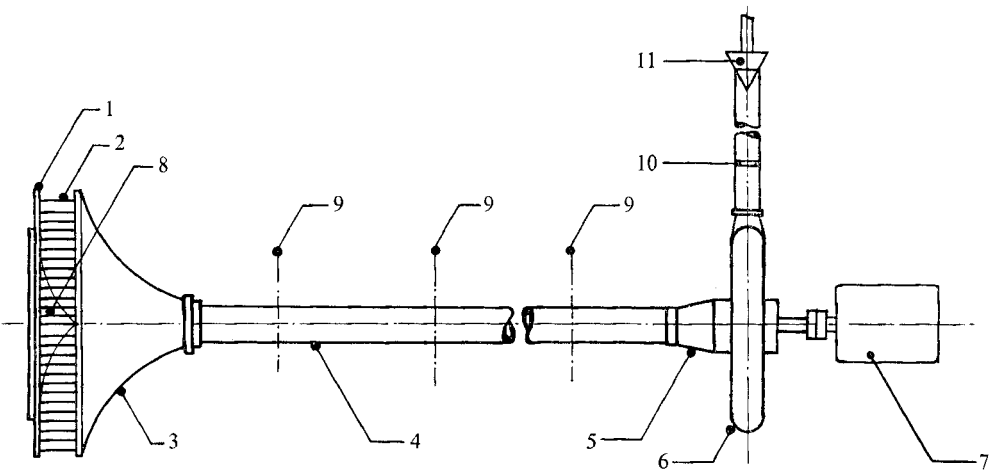

FIGURE 1. Experimental set-up. 1, turning mechanism; 2, swirl vanes; 3, entry section; 4, perspex duct; 5, flexible connexion; 6, blower; 7, motor; 8, cone; 9, test stations; 10, orifice meter; 11, adjustable end resistance.

2. Apparatus and experimental procedure

2.1. *General*

The apparatus consisted essentially of a pipe with a length of approximately 100 diameters connected to an entry section on the upstream side and a centrifugal blower and an orifice meter on the downstream side (figure 1). The initial swirl was controlled by adjustable guide vanes in the entry section, and the flow rate was controlled by an adjustable end resistance at the outlet of the orifice meter. A maximum Reynolds number Re (based on the pipe diameter and average velocity) of $2{\cdot}6 \times 10^5$ could be obtained. Also, a maximum angle between the local mean velocity at the central station and the pipe axis of 15° was obtainable.

Mean velocity profile measurements were carried out using standard probes at three stations I, II and III at 25, 50 and 75 diameters from the entry section. Several methods of measuring the local axial skin friction were tried. Their effectiveness is discussed in § 4.

2.2. *Details of the apparatus*

Two transparent perspex pipes of length 6 m, internal diameter 120·5 mm, and wall thickness 3 mm were used in the apparatus. Variations in pipe diameter were within about one per cent. The two pipes were carefully connected and held on a rigid frame.

The wooden contraction cone of the entry section (figure 2, plate 1) had a surface of revolution generated by a cubic curve. Two disks of diameter 86 cm spaced 13 cm apart guided the incoming air, giving a contraction ratio of 30. There were 72 guide vanes of chord 18 cm at a circumferential pitch of 3·6 cm which could be turned equally by a specially designed mechanism. Guide vanes have several advantages over other types of swirl generators. Unlike twisted tape or coiled

wire, they do not create secondary flows. Departures from rotational symmetry can be reduced by increasing the number of vanes. Continuous control of the initial swirl provided by the vanes may be useful in some experiments.

A centrifugal blower was connected at the downstream end through a flexible connexion. After extensive checks and modifications, a steady drift and vibration-free operation could be obtained over several hours.

Earlier studies (Nigam 1970; Yajnik & Subbaiah 1971) were carried out in the same apparatus, but with another entry section and a slightly different test section. Some representative data from these studies, shown by flagged symbols, are included here, mainly to show that the observations are not sensitive to details of initial conditions.

2.3. *Unsteadiness in presence of swirl*

In the early stages, unsteadiness was observed in the central region of the pipe, particularly near the entry section, probably owing to unsteady separation on the end disk of the entry section. A cone with a cubic profile was designed to stabilize the flow and to provide a gradual reduction in cross-sectional area (figure 2). Unsteadiness was markedly diminished after the installation of the cone.

2.4. *Probes and their calibration*

A five-holed conical-head probe of diameter 6 mm was first made for the three-dimensional flow measurements, particularly near the entry section. Velocity profile measurements at station I indicated that the maximum radial velocity was less than about 1 % of the axial velocity for swirl angles up to 15°. Since most of the measurements were carried out in this range of swirl angle, a simpler two-dimensional probe was used in further measurements. The three-tube probe was carefully made from stainless-steel tubes of 0·45 mm inner and 0·82 mm outer diameter, the chamfer angle being 45°. A null type of calibration (Bryer, Walshe & Garner 1958) obtained in a 90×60 cm tunnel yielded a calibration curve which was well approximated by a linear relation $q = K(p_0 - p_1)$, p_0 and p_1 being central and side tube pressures. K was found by a least-squares fit.

Velocity profiles were measured with cobra and pitot probes in pipe flow without swirl at several Reynolds numbers. A typical comparison given in figure 3 shows that the errors due to using uniform-flow calibration are acceptably small.

3. Swirl parameter

Early studies described swirl in terms of the geometrical parameters of the swirl generating device like the pitch-to-diameter ratio H/D of a twisted tape or the inlet guide vane angle. An interesting example of this type of parameter is a Dean number based on twisted-tape geometry (Shchukin 1967). Such parameters however do not facilitate the comparison of data obtained with different types of generators. Further, they often describe the initial swirl rather than swirl at a downstream section.

The angular velocity of a freely turning vane located at a given section de-

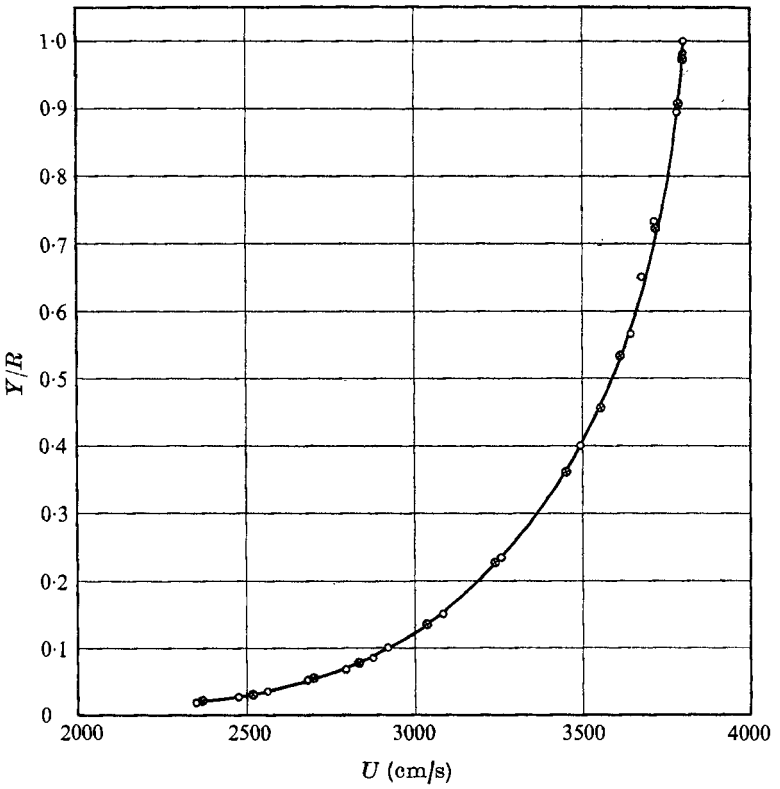

FIGURE 3. Axial velocity profile for zero-swirl flow at $Re = 2{\cdot}59 \times 10^5$. ○, with three-tube probe; ⊗, with pitot static probe.

scribes the swirl at the section in some average sense. This measure has been successfully used in studies on swirl decay (Kreith & Sonju 1965). The device needs calibration and possibly interference studies. Also, the use of a vane at a section is not convenient if velocity profile measurements are desired at the same section.

Another measure of swirl, which will be called the swirl number S, can be defined in terms of angular and axial momentum fluxes associated with the mean flow as

$$S = \int_0^R UVr^2 dr \Big/ R\int_0^R U^2 r\, dr. \tag{1}$$

Here U and V are the axial and tangential components of the mean velocity at a given section at a point a distance r from the axis and R is the pipe radius. The swirl number has the major conceptual advantage of possessing a clear physical meaning.

A somewhat similar quantity S' has also been used:

$$S' = \int_0^R UVr\, dr \Big/ \int_0^R U^2 r\, dr. \tag{2}$$

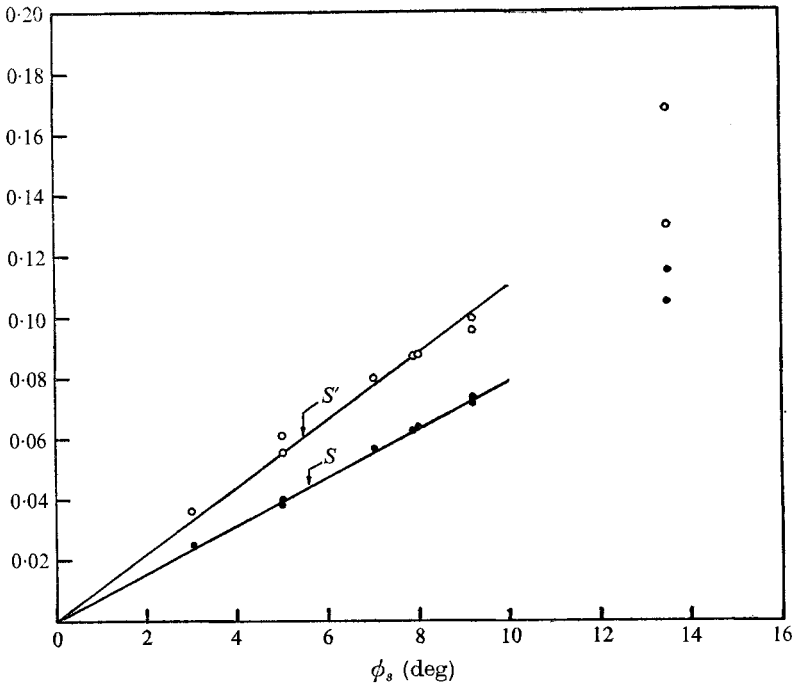

FIGURE 4. Variation of swirl angle with swirl number.
●, S; ○, S'. $S = 0{\cdot}0079\phi_s$ and $S' = 0{\cdot}011\phi_s$.

However, the integral in the numerator, which is termed the 'tangential momentum flux', makes the quantity difficult to interpret.†

If we define an axial velocity scale U_a and an angular velocity scale Ω by

$$\left.\begin{aligned} \pi\rho U_a^2 R^2 &= 2\pi\int_0^R \rho U^2 r\,dr, \\ \pi\rho U_a \Omega R^4 &= 2\pi\int_0^R \rho U V r^2 dr \end{aligned}\right\} \tag{3}$$

the swirl number is seen to be $\Omega R/U_a$, or the inverse of the well-known Rossby number. If other scales are used in defining the Rossby number, its relationship with the swirl number may not remain so direct and may also involve the Reynolds number.

It was realized during the course of the experiments that a parameter which does not involve integrals would offer considerable operational advantages. The flow angle ϕ is the angle between the pipe axis and the mean flow direction.

† Vr is the component of angular momentum per unit mass in the axial direction for all points in a section, but V is a component of momentum per unit mass in a direction which varies from point to point at a section. Hence it is difficult to attach any significance to an integral like

$$\int_0^R UVr\,dr.$$

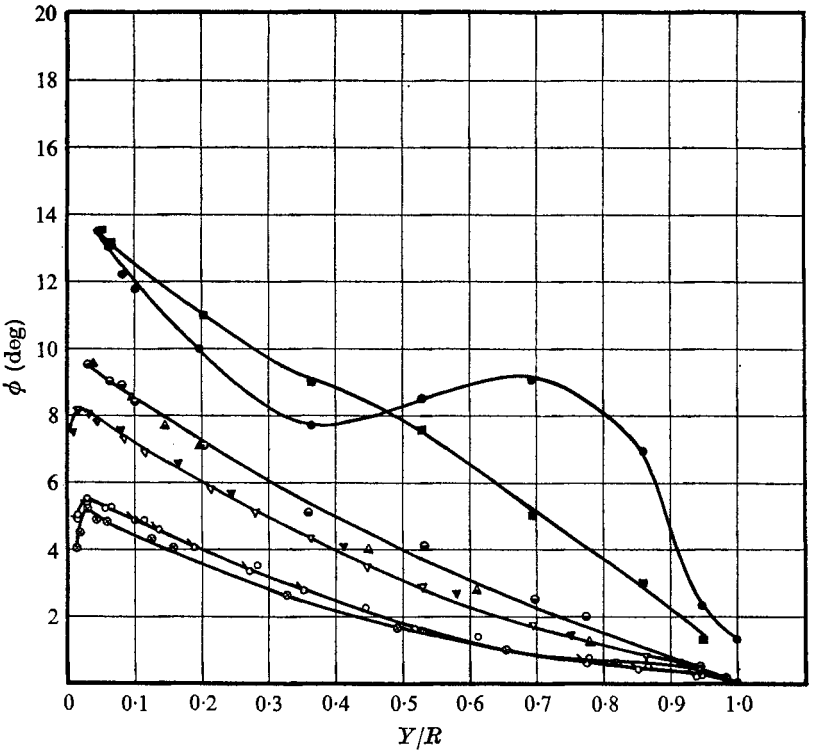

FIGURE 5. Inclination of velocity.

Symbol	ϕ_s	Re	Station
⊗	5°	$1{\cdot}4 \times 10^5$	II
◔	5°	$1{\cdot}42 \times 10^5$	II
○	5°	$1{\cdot}36 \times 10^5$	III
▼	8·0°	$2{\cdot}35 \times 10^5$	II
▽	7·9°	$2{\cdot}37 \times 10^5$	III
▲	9·2°	$0{\cdot}67 \times 10^5$	II
◒	9·2°	$2{\cdot}48 \times 10^5$	II
●	13·5°	$2{\cdot}36 \times 10^5$	II
■	13·5°	$0{\cdot}67 \times 10^5$	II

A reference point was selected at 5 % of the pipe radius from the wall† and the corresponding flow angle is called the swirl angle ϕ_s in subsequent sections.

Figure 4 shows the variation of the swirl number with the swirl angle for stations I, II and III and for several Reynolds numbers. Since all points, except those for $\phi_s = 13{\cdot}5°$, lie practically on a straight line, S is completely determined by ϕ_s for the present experiments. The exceptional points are discussed later. Similarly S' is also completely determined to a first approximation by ϕ_s.

Figure 5 shows flow-angle ϕ profiles for several flow rates. When the vane angle and the flow rate were changed without changing ϕ_s, ϕ profiles away from

† At this location, ϕ was close to its maximum value ϕ_m, which also could be used as a swirl measure. However, for geometrical reasons the measurement of flow angles very close to the wall was not possible.

the wall and the swirl number did not change except in one case, when ϕ_s was 13·5°. Unusual variations were also observed in the tangential velocity profiles for the exceptional case (figure 13), which was found to be associated with flow reversal near the entry section. The similarity studies were carried out for a range of initial conditions which excluded flow reversal. Since ϕ_s determines S under the experimental conditions, it may be used to characterize swirl at a station.

Use of the swirl angle resulted in considerable experimental facility. For instance, changes in the Reynolds number keeping ϕ_s constant were brought about by keeping the three-tube probe at $Y/R = 0{\cdot}05$ in the direction ϕ_s and by changing the flow rate and the initial vane angle until the flow direction coincided with the probe direction. Since the swirl number involves integrals, changes in the Reynolds number keeping S fixed would require a trial-and-error procedure involving several profile measurements.

4. Measurement of skin friction

Measurement of skin friction in three-dimensional flow is well-known to have attendant difficulties (e.g. Brown & Joubert 1969). Since a certain amount of uncertainty was unavoidable, two methods were used with extensive checks with and without swirl. These checks, some of which are reported in the next section, give us confidence in the measured skin-friction values.

The mean flow direction close to the wall was inclined at an angle less than about 15° to the pipe axis at the stations in the range of the present experiments. Hence, the tangential skin friction was expected to be much smaller than the axial component. Attention was therefore focused on the measurement of the latter.

A common method of measurement relates the axial skin friction to the pressure drop by the relation

$$C_f = \tau_w/\tfrac{1}{2}\rho U_{\mathrm{av}}^2 = \Delta p/(2\rho U_{\mathrm{av}}^2 L/D) = \tfrac{1}{4}\lambda. \tag{4}$$

U_{av} is the cross-sectional average of the axial mean velocity, τ_w is the wall shear stress, ρ is the fluid density, λ is the axial skin-friction coefficient and D is the inner diameter of the pipe. The static pressure drop Δp is over a horizontal length L. If there is a radial pressure gradient, Δp has to be some average measure of the difference in static pressure between the initial and final sections. Most skin-friction data reported in the literature on swirling pipe flow use the above relation. The static pressure is usually measured by wall taps separated by a distance of the order of 50 diameters.

The above relation is exact if the axial momentum fluxes at the two sections are equal and the skin friction is uniform over the length L. While these conditions are satisfied in fully developed zero-swirl pipe flow, swirl introduces three effects which give rise to errors. First, the decay of swirl leads to variations in skin friction and hence the average skin-friction coefficient given by the above relation, in general, differs from the local skin-friction coefficient at the midway section. Second, the axial velocity profile changes with the decay of swirl and

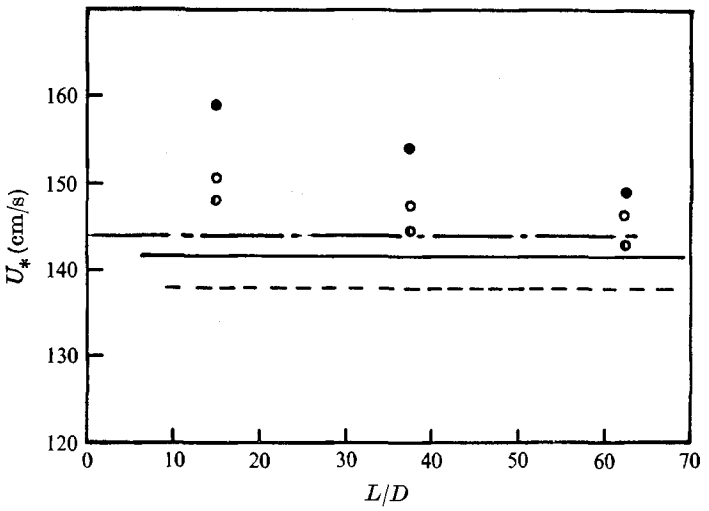

FIGURE 6. Comparison of friction velocities obtained by three methods. No swirl, station II: ●, from Δp measured using wall taps; ◐, from Δp measured using static heat probes; ——, by Bradshaw's method; – – , estimate from Ludwig Tillmann formula. $\phi_s = 9{\cdot}2°$, station II: ○, from Δp measured using static head probes; —·—, by Bradshaw's method.

the momentum fluxes at the initial and final sections are generally different, although the difference is expected to be small. Third, the presence of the radial pressure gradient which accompanies swirl may make the average pressure drop slightly different from the drop measured at the wall or at a chosen radius. In addition, there is the usual entry-length effect.

Figure 6 shows skin-friction values obtained from the wall taps for three values of L/D. The taps were located symmetrically about station II. A slight drop in the measured skin friction with increasing L/D was a typical feature found at all Reynolds numbers and swirl conditions. Since the taps were in a 6 m long pipe, the geometry was difficult to control, which might have led to errors in the measurement of the static pressure drop (Rayle 1949). Hence, static pressure probes were used at the initial and final sections at a distance of half the pipe radius from the axis. When swirl was present, they were aligned in the flow direction found by the three-tube probe. Skin-friction values obtained by this method were lower than the earlier set and the trend for a slight decrease with increases in L/D was also present. These values are regarded as more accurate than the wall tap readings.

Methods based on wall similarity form another important class. If it is assumed that the axial velocity in the wall co-ordinates follows a logarithmic law in the overlap region with friction velocity defined in terms of the axial skin friction and if the coefficients of the law are known *a priori*, the method of Clauser (1954) or Bradshaw (1959) can be used. Bradshaw's method was adopted for its known simplicity.

Figure 6 compares the values obtained by this method with those from the other two methods. The values obtained from static pressure probes agreed with those obtained by Bradshaw's method to a greater extent than the values from

wall tap measurements. Also, comparisons for the swirl case showed a similar trend. (A typical estimate based on the Ludwig Tillman formula is also given in figure 6 for the zero-swirl case.)

While other methods based on wall similarity could be used, they were not seriously tried. Some of them seemed to have disadvantages for the present problem. For instance, the Preston tube has to be aligned along the pipe axis and the tangential velocity would lead to certain additional averaging errors.

It has also to be pointed out that the general form for wall similarity for three-dimensional flows has not been definitely established. But since the flow direction close to the wall differs from the axial direction by less than 15°, errors of this type are not likely to exceed 5 %.

Values based on Bradshaw's method were used for the scaling of the wall and defect laws considered in §6. They were found to give internally consistent results.

5. Flow away from entry

Several options are available for describing the flow away from the entry section when flow reversal is absent and it is advantageous to discuss them before discussing the results of the experiments. Our interest is in the region away from the entry section, where the geometrical and dynamic details of the entry conditions do not have significant consequences. At the same time, if the mode of description for large distances is such that common pipe lengths used in the laboratory or applications are not sufficient, then such a mode is of little interest.

The simplest mode of description is a fully developed flow, which may be defined as a state in which the axial and tangential velocity profiles, Reynolds stress profiles and mean pressure gradient do not change with the axial distance. The invariance of the tangential velocity implies an invariant angular momentum flux. Since the tangential component of pipe skin friction goes on decreasing the angular momentum flux, such a state is asymptotically attained after the swirl has decayed to insignificant levels. This flow is identical with the well-known zero-swirl flow. Also, the experiments clearly show that swirl persists over lengths of the order of 100 diameters, which would normally be used in the laboratory or applications. Hence such a notion of fully developed flow is not useful for the present problem.

Another mode would be local similarity, according to which the mean flow profiles at a section are completely determined in terms of certain properties of the flow at the section. These properties can be used as local parameters to describe the flow and no additional information about initial conditions is required. This mode of description has been successfully used in other turbulent shear flows (e.g. Townsend 1956, p. 89) and is adopted here.†

Still another mode would be a state in which the initial conditions influence the flow through certain gross parameters, but the details of the initial conditions

† As the local parameters may change with axial distance, the velocity profiles may also change their shape and need not be geometrically similar. Another point to note is that the changes in the local parameters with axial distance may depend on initial conditions.

Run number	S	ϕ_s	$Re \times 10^{-5}$	Station
1	0	0	1·5	II
2	0	0	2·57	I
3	0	0	2·59	II
4	0·025	3°	1·56	II
5	0·038	5°	1·4	II
6	0·04	5°	1·42	II
7	0·039	5°	1·36	III
8	0·041	5°	2·4	I
9	0·055	6·8°	1·2	III
10	0·056	7°	2·39	III
11	0·063	7·9°	2·37	III
12	0·064	8°	2·38	I
13	0·063	8°	2·35	II
14	0·071	9·2°	0·42	II
15	0·0715	9·2°	0·67	II
16	0·073	9·2°	2·48	II
17	0·177	13·0°	2·4	I
18	0·105	13·5°	0·67	II
19	0·155	13·5°	2·36	II
20	—	—	2·4	I

TABLE 2. Summary of parameters for test runs. Streamwise turbulent intensity and spectrum measurements also were made for runs 3, 16 and 19. Runs 19 and 20 are for the same initial swirl and Reynolds number, the velocity profile data of the latter being incomplete on account of flow reversal. Runs 11, 16 and 17 correspond to the same initial vane setting and approximately the same Reynolds number.

are of no consequence. For instance, a swirling flow in such a state may be governed by the initial angular momentum but not by the shape of the initial tangential velocity profile. Distance from a virtual origin is an example of this type of parameter which is used in some shear flows.

These modes correspond to leading terms of asymptotic expansions for large axial distance. Similarity representations discussed in the next section are the leading terms of one type of expansion.

The small perturbation approach of Talbot deals with a perturbation of the fully developed state. It calls for an expansion in a small parameter governing the initial perturbation. If we consider a two-term co-ordinate expansion corresponding to the first mode, we get similar equations, but they describe the final stages of decay of angular momentum, unlike the initial-value problem considered by Talbot.

6. Results and discussion†

6.1. *Wall region*

Figure 7 shows axial velocity profiles in wall co-ordinates.‡ The origins are shifted for clarity. Zero-swirl measurements are seen to be in good agreement with the

† Table 2 gives important parameters of the test runs. Figures show only representative data from the runs for the sake of clarity.

‡ Measurements were largely restricted to $YU_*/\nu > 80$ for geometrical reasons, where U_* is axial friction velocity and ν is the kinematic viscosity of air.

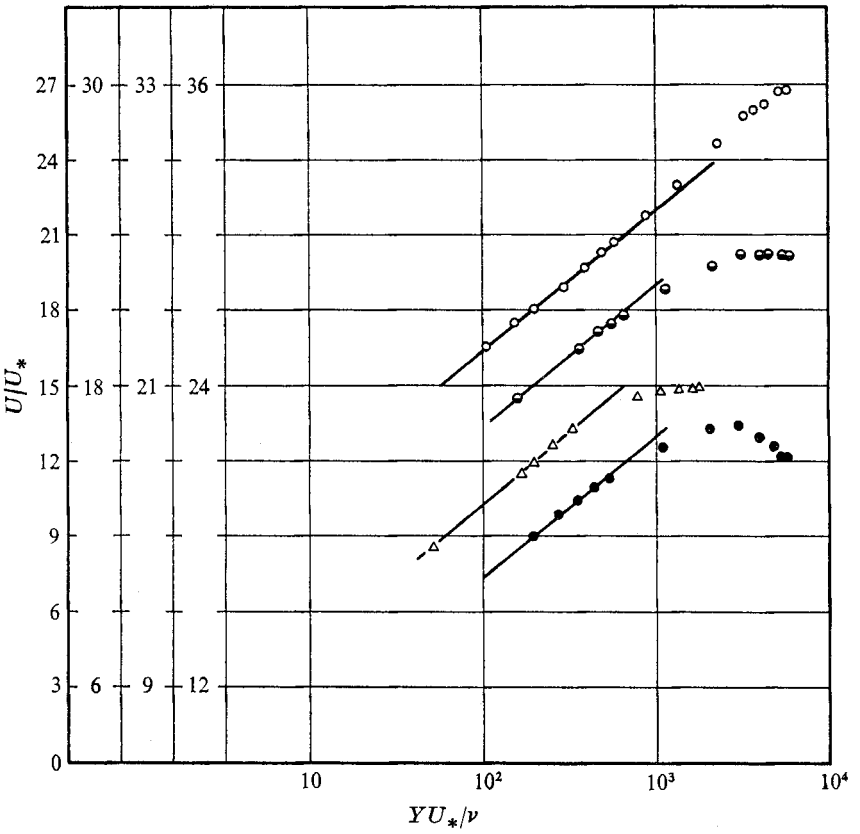

FIGURE 7. Axial velocity profiles in wall co-ordinates (station II). ○, no swirl, $Re = 2{\cdot}59 \times 10^5$; △, $\phi_s = 9{\cdot}2°$, $Re = 0{\cdot}67 \times 10^5$; ◒, $\phi_s = 9{\cdot}2°$, $Re = 2{\cdot}48 \times 10^5$; ●, $\phi_s = 13{\cdot}5°$, $Re = 2{\cdot}36 \times 10^5$; ——, logarithmic law $U/U_* = k^{-1}\ln(YU_*/\nu) + A$, with $k = 0{\cdot}41$ and $A = 5{\cdot}2$.

logarithmic law in the overlap region. When swirl is present, the profiles in the overlap region continue to obey the logarithmic law. The range over which the profile is logarithmic depends on the Reynolds number and swirl. Hence the extent of the wall region may depend on the swirl, but within this region, the wall law in the overlap region does not show any detectable effect of swirl.

Since Bradshaw's method, which assumed wall similarity, was used for finding the friction velocity U_*, the reasoning may appear circular. But the pressure-drop methods which do not assume wall similarity also gave values of the skin friction close to the values used here, as discussed in §4. Further, since the flow direction makes an angle of less than 15° with the pipe axis, the observations would also be compatible with slightly different similarity representations (for instance, one obtained by using the velocity component in the direction of the skin friction rather than the axial component).

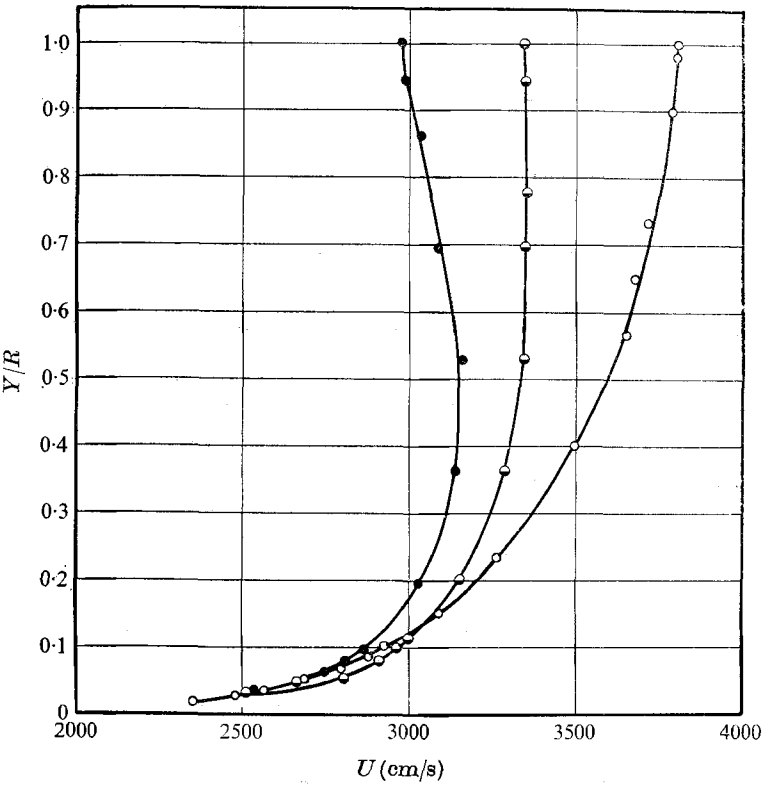

FIGURE 8. Axial velocity profiles (station II). ○, no swirl, $Re = 2{\cdot}59 \times 10^5$; ◒, $\phi_s = 9{\cdot}2°$, $Re = 2{\cdot}48 \times 10^5$; ●, $\phi_s = 13{\cdot}5°$, $Re = 2{\cdot}36 \times 10^5$.

6.2. *Core region*

The typical axial velocity profiles with swirl given in figure 8 show that the maximum velocity need not occur at the pipe axis. As the swirl increases, the maximum velocity location shifts from the axis, giving rise to a valley in the velocity profile. Clearly, with a further increase in swirl, negative axial velocities would appear near the axis.

If the normalized axial velocity (U/U_{av}) profile depends only on ϕ_s and Re, profiles obtained for two initial swirls at two different stations would collapse onto each other, provided ϕ_s and Re had the same values at the two stations. Figure 9 shows that this condition is satisfied.

A similarity represention of the velocity defect allows the Reynolds number to vary. Normally, the velocity defect is defined as $U_0 - U$, where U_0 is the velocity at the pipe axis. It is however convenient for our purpose to use $U - U_{\mathrm{av}}$ as a measure of the velocity defect, since U_{av} is measured more accurately than U_0. Also, the translation effect on the velocity defect profile produced by the sensitivity of U_0 makes it difficult to isolate other effects.

U_{av} was found by numerical integration of the measured axial velocity profile. It was checked by comparing the average value with that of the orifice meter. Agreement was typically within 3 %.

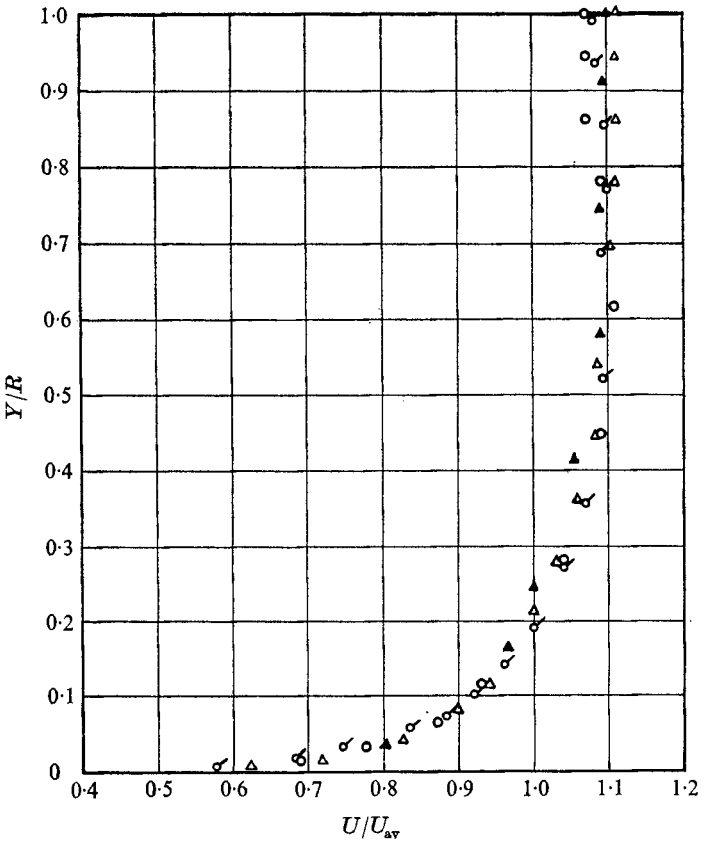

FIGURE 9. Axial velocity profile. ♂, $\phi_s = 5{\cdot}0°$, $Re = 1{\cdot}42 \times 10^5$, station II; ○, $\phi_s = 5{\cdot}0°$, $Re = 1{\cdot}36 \times 10^5$, station III; ▲, $\phi_s = 8{\cdot}0°$, $Re = 2{\cdot}35 \times 10^5$, station II; △, $\phi_s = 7{\cdot}9°$ $Re = 2{\cdot}37 \times 10^5$, station III.

The velocity defect profiles shown in figure 10 indicate the nature of the similarity in the core region. When the initial swirl was altered and the Reynolds number was also altered to keep the swirl angle at a given station constant, the velocity defect profile did not change significantly. Further, when velocity defect profiles measured at two stations, II and III, were compared for two different runs whose initial swirl and Reynolds numbers were adjusted to produce the same swirl angle, no significant change was observed in the core region.

Velocity defect profiles are shown on a logarithmic scale in figure 11 without an origin shift, and they indicate another effect of swirl. The profile remains logarithmic in the overlap region and there is no significant variation of the slope of the semi-log plot. But the curve is steadily dislpaced upwards with increasing swirl. The additive coefficient B of the defect logarithmic law is thus dependent on the swirl angle ϕ_s. Figure 16 shows that the coefficient B varies approximately linearly with ϕ_s.

The velocity defect profiles (figure 11) fall below the logarithmic law as the pipe axis is approached. This behaviour is in contrast to zero-swirl behaviour

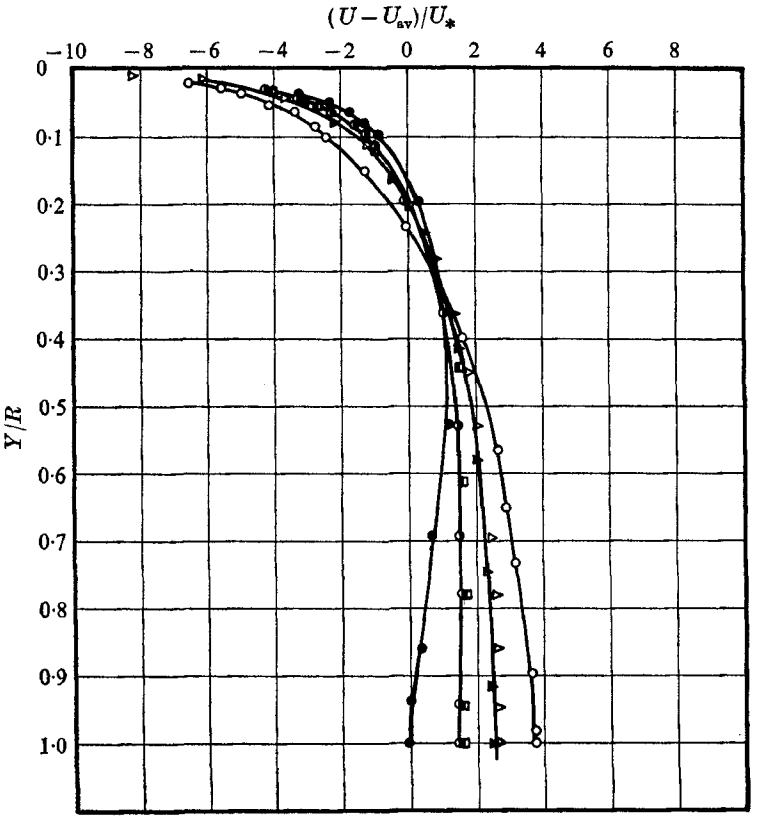

FIGURE 10. Axial velocity defect profiles. ○, no swirl, $Re = 2{\cdot}59 \times 10^5$, station II; △, $\phi_s = 7{\cdot}9°$, $Re = 2{\cdot}36 \times 10^5$, station III; ▲, $\phi_s = 8{\cdot}0°$, $Re = 2{\cdot}35 \times 10^5$, station I; ⬓, $\phi_s = 9{\cdot}2°$, $Re = 0{\cdot}42 \times 10^5$, station II; ◒, $\phi_s = 9{\cdot}2°$, $Re = 2{\cdot}48 \times 10^5$, station II; ●, $\phi_s = 13{\cdot}5°$, $Re = 2{\cdot}36 \times 10^5$, station II.

and it can also be seen from figure 8. Swirl may then be said to give rise to a 'negative wake component'.

Following the definition of Coles (1956),

$$U/U_* = f(YU_*/\nu) + \Pi k^{-1} W(Y/\delta), \tag{5}$$

where Π is a profile parameter and W the wake function. $W(Y/\delta)$, subject to the normalizing conditions

$$\max |W(Y/\delta)| = W(1) = 2, \tag{6}$$

is plotted in figure 12. The experimental points show fair agreement with the universal wake function proposed by Coles.

Tangential velocity profiles are plotted in figure 13. They clearly show that, when the flow angle at a section is maintained constant and the initial swirl is varied, tangential velocity profiles do not change. The profile for the swirl angle of 13·5° has flow reversal at station I and will be discussed in part 2. The shape of the tangential velocity profiles is similar to those given in earlier investigations.

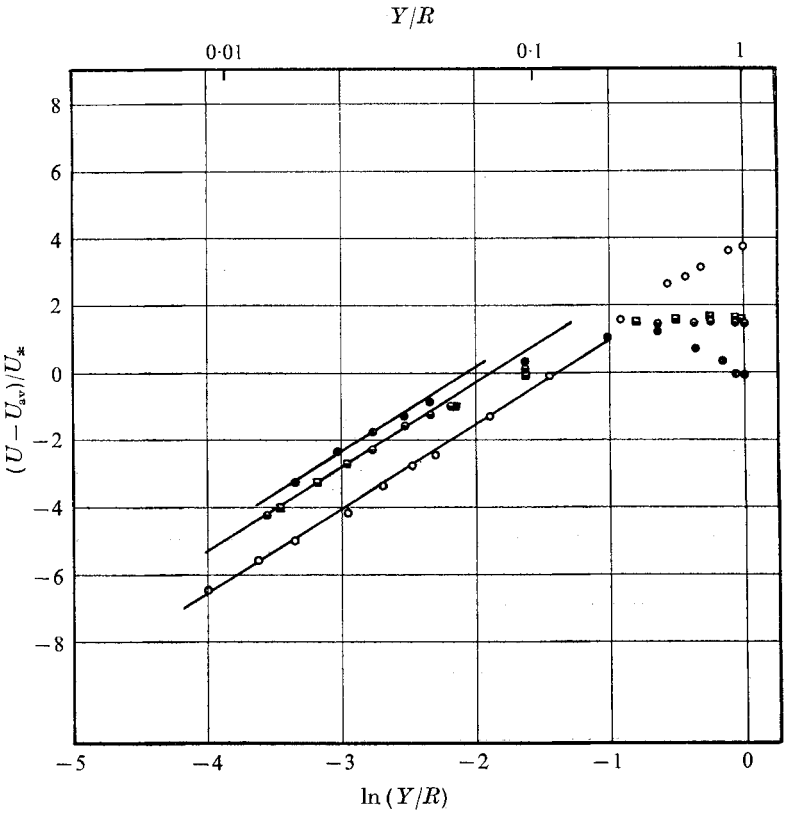

FIGURE 11. Axial velocity defect in overlap region. ○, no swirl, $Re = 2{\cdot}59 \times 10^5$; ◒, $\phi_s = 9{\cdot}2°$, $Re = 0{\cdot}42 \times 10^5$; ◒, $\phi_s = 9{\cdot}2°$, $Re = 2{\cdot}48 \times 10^5$; ●, $\phi_s = 13{\cdot}5°$, $Re = 2{\cdot}36 \times 10^5$.

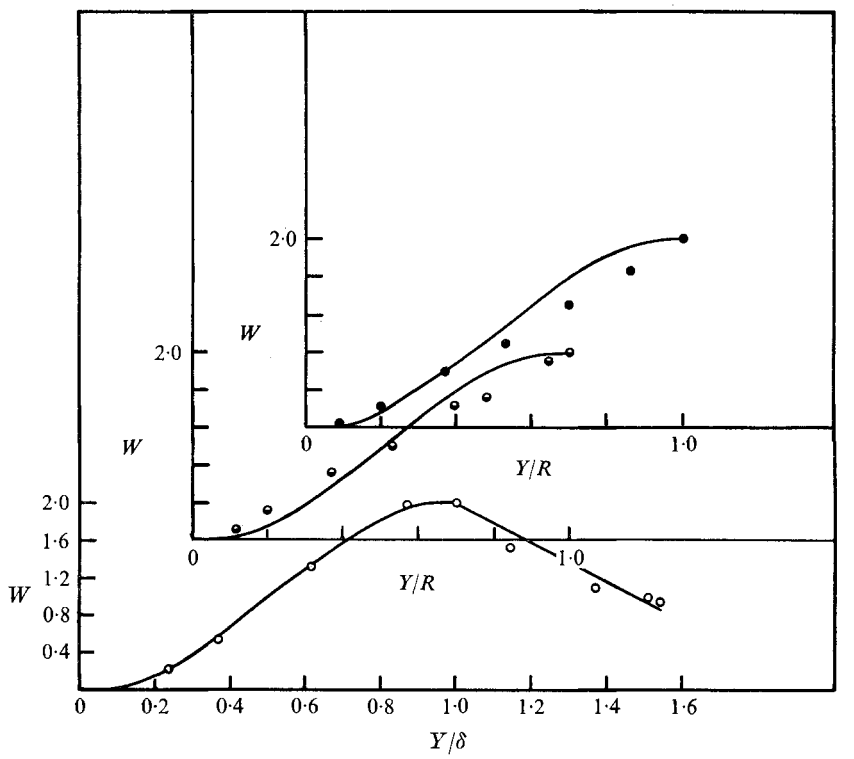

FIGURE 12. Wake function. ○, no swirl, $Re = 2{\cdot}59 \times 10^5$; ◒, $\phi_s = 9{\cdot}2°$, $Re = 2{\cdot}48 \times 10^5$; ●, $\phi_s = 13{\cdot}5°$, $Re = 2{\cdot}36 \times 10^5$.

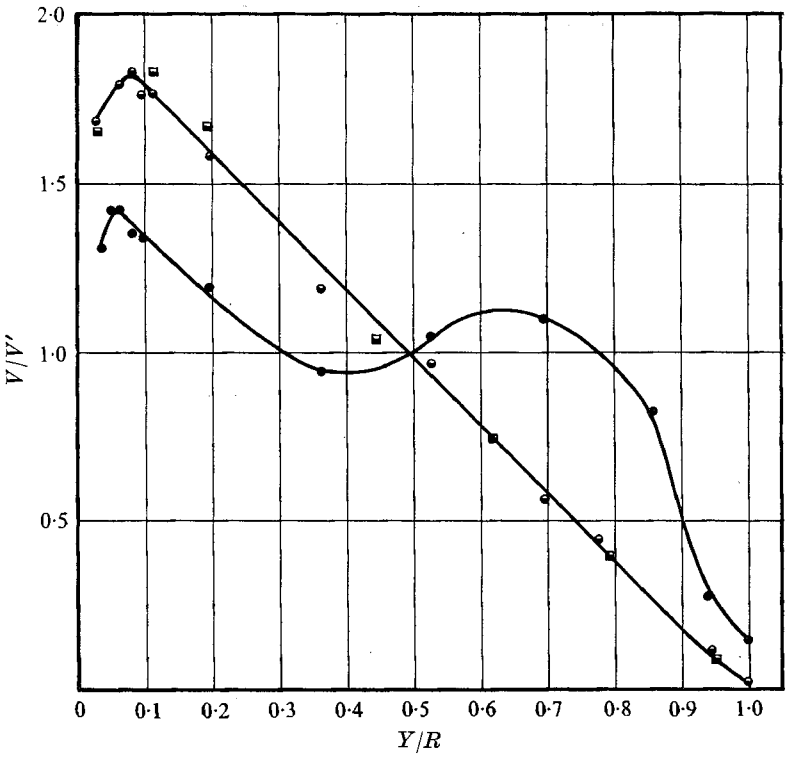

FIGURE 13. Tangential velocity profiles. ◒, $\phi_s = 9{\cdot}2°$, $Re = 2{\cdot}48 \times 10^5$; ◘, $\phi_s = 9{\cdot}2°$, $Re = 0{\cdot}42 \times 10^5$; ●, $\phi_s = 13{\cdot}5°$, $Re = 2{\cdot}36 \times 10^5$. V' is the tangential velocity at $Y/R = 0{\cdot}5$.

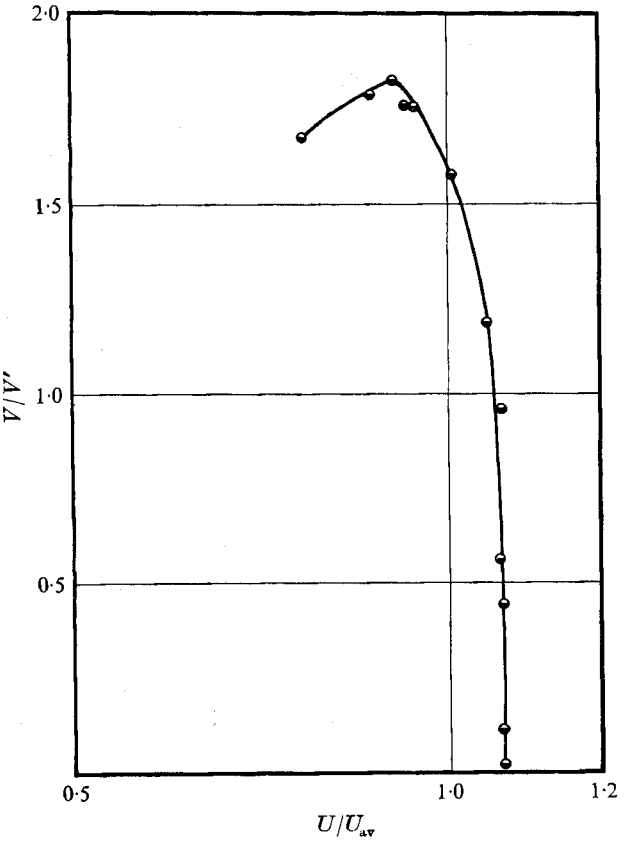

FIGURE 14. Johnson plot. $\phi_s = 9{\cdot}2°$, $Re = 2{\cdot}48 \times 10^5$, station II.

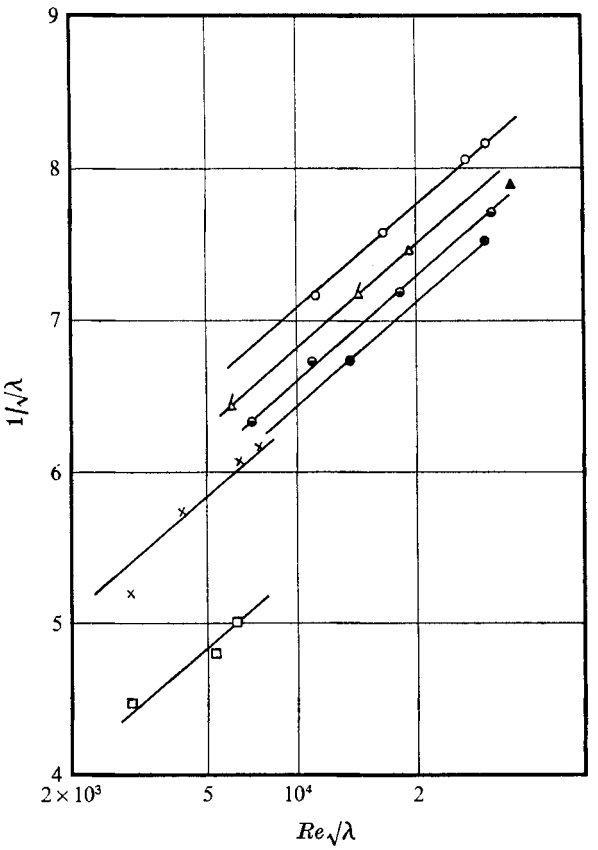

FIGURE 15. Axial skin-friction law. ○, no swirl; △, ▲, $\phi_s = 5°$; ▲, $\phi_s = 8°$; ◒, $\phi_s = 9{\cdot}2°$; ●, $\phi_s = 13{\cdot}5°$; ×, Smithberg & Landis (1964), $H/D = 10{\cdot}3$; □, Koch (1958), $H/D = 5{\cdot}0$.

To show how the variation of flow direction compares with three-dimensional turbulent boundary layers, velocity vectors were plotted in a Johnson plot (figure 14). Clearly, the general trend is similar, but with increasing swirl, the slope becomes very steep near the axis and the peak becomes increasingly rounded.

6.3. *Skin-friction law*

Figure 15 shows a semi-logarithmic plot of $1/\sqrt{\lambda}$ *vs.* $Re\sqrt{\lambda}$. λ was measured by Bradshaw's method and, as mentioned earlier, is close to the value obtained from pressure-drop measurements. The present results are compatible with the well-established law in absence of swirl. If the swirl angle ϕ_s at a section is increased, the curve retains its linear character and is displaced downwards, indicating an increase in the local skin friction.

The earlier data are not strictly comparable as they refer to average values of the skin friction and the swirl is specified differently. But figure 15 shows that the same trend can be found in the data of Smithberg & Landis (1964) and Koch (1958).

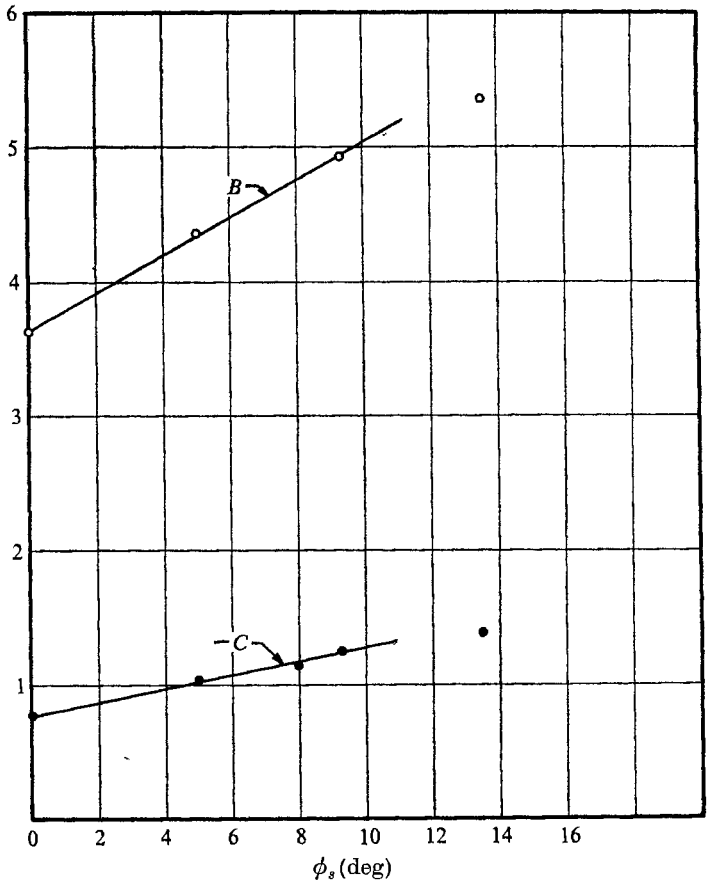

FIGURE 16. Effect of swirl on the additive coefficients in the logarithmic skin-friction law and velocity defect law in overlap region.

If, at sufficiently large Reynolds numbers, the following representations hold in the overlap region:

$$U/U_* = k^{-1}\ln(YU_*/\nu)+A,$$

$$(U-U_{\mathrm{av}})/U_* = k^{-1}\ln(Y/R)+B,$$

then
$$1/\sqrt{\lambda} = (\tfrac{1}{2}\sqrt{\tfrac{1}{2}}k)\ln(Re\sqrt{\lambda})+C,$$

where
$$C = [A-B-k^{-1}\ln 4\sqrt{2}]/2\sqrt{2}. \qquad (7)$$

Here the coefficients B and C may depend on ϕ_s. Thus the observations of the velocity profile in the overlap region imply a logarithmic skin-friction law whose additive coefficient depends on the swirl angle.

Figure 16 shows the variation of the coefficients B and C with the swirl angle. The former is obtained from the logarithmic velocity defect law and the latter from the logarithmic skin-friction plot. In both cases, least-square fits were used. Clearly, the coefficients vary linearly with the swirl angle in the range of the

present experiments. Using a least-squares fit, we find that the following correlations fit the present measurements to a good approximation:

$$B = 3{\cdot}60 + 0{\cdot}14\phi_s, \quad C = -0{\cdot}77 - 0{\cdot}05\phi_s.$$

The ratio of the slopes of the two curves for B and C *vs.* ϕ_s is found to be $-2{\cdot}9$. The relation (7) implies a ratio of $-2\sqrt{2}$. This close agreement supports the view that similarity representations are good approximations under the conditions of the experiment. It also provides an indirect indication of the accuracy of measurements.

REFERENCES

BINNIE, A. M. 1957 Experiments on the slow swirling flow of a viscous liquid through a tube. *Quart. J. Mech. Appl. Math.* **10**, 276–290.

BINNIE, A. M. & TEARE, J. D. 1956 Experiments on the flow of swirling water through a pressure nozzle and an open trumpet. *Proc. Roy. Soc.* A **235**, 78–79.

BRADSHAW, P. 1959 A simple method of determining turbulent skin friction from velocity profiles. *J. Aerospace Sci.* **26**, 841.

BROWN, K. C. & JOUBERT, P. N. 1969 The measurement of skin friction in turbulent boundary layers with adverse pressure gradients. *J. Fluid Mech.* **35**, 737–757.

BRYER, D. W., WALSHE, D. E. & GARNER, H. C. 1958 Pressure probes selected for three-dimensional flow measurement. *Aero. Res. Counc. R. & M.* no. 3037.

CLAUSER, F. H. 1954 Turbulent boundary layers in adverse pressure gradients. *J. Aero. Sci.* **21**, 91–108.

COLES, D. 1956 The wake in the tubulent boundary layer *J. Fluid Mech.* **1**, 191–226.

GORE, R. W. & RANZ, S. E. 1964 Back flows in rotating fluids moving axially through expanding cross sections. *A.I.Ch.E. J.* **10**, 83–88.

KINNEY, R. B. 1967 Universal velocity similarity in fully turbulent rotating flow. *J. Appl. Mech., Trans. A.S.M.E.* **89** (3), 437–442.

KIYA, M., FUKUSAKO, S. & ARIE, M. 1971 Laminar swirling flow in the entrance region of a circular pipe. *Bull. Japan Soc. Mech. Engng*, **14**, 659–670.

KOCH, R. 1958 Druckverlust and Wärmeübergang bei verwirbelter, Strömung. *VDI-Forschungsheft*, B**24**, 469.

KRAUSE, E. & HIRSCHEL, E. H. (eds.) 1970 Strömungsmechanische Vorgänge in Gaszentrifugen. *DFVLR-Colloq. Porz-Wahn, Inst. angew. Gasdynamik.*

KREITH, F. & MARGOLIS, D. 1959 Heat transfer and friction in turbulent vortex flow. *Appl. Sci. Res.* A **8**, 457–468.

KREITH, F. & SONJU, O. K. 1965 The decay of turbulent swirl in a pipe. *J. Fluid Mech.* **22**, 257–271.

LAVAN, Z., NIELSEN, H. & FEJER, A. A. 1969 Separation and flow reversal in swirling flows in circular ducts. *Phys. Fluids*, **12**, 1747–1757.

MAGER, A. 1971 Incompressible viscous swirling flow through a nozzle. *A.I.A.A. J.* **9**, 649–655.

MIGAY, V. K. & GOLUBEV, L. K. 1970 Friction and heat transfer in turbulent swirl flow with a variable swirl generator in a pipe. *Heat Transfer, Sov. Res.* **2**, 68–73.

NIGAM, A. 1970 Some experiments in swirling pipe flow. M. Tech. thesis. Ind. Inst. Tech., Kanpur.

NUTTAL, J. B. 1953 Axial flow in a vortex *Nature*, **172**, 528–583.

RAYLE, R. E. 1949 An investigation of the influence of orifice geometry on static pressure measurements. SM thesis, Dept. of Mech. Engng., M.I.T.

ROCHINO, A. P. & LAVAN, Z. 1969 Analytical investigation of incompressible turbulent swirling flow in pipes. *J. Appl. Mech.* **36**, 151–158.

SACHDEVA, R. C. 1968 An experimental investigation of swirling flow through a pipe. M. Tech. thesis, Ind. Inst. Tech., Kanpur.

SENOO, Y. & NAGATA, T. 1972 Swirl flow in long pipes with different roughness. *Bull. Japan Soc. Mech. Engng*, **15**, 1514–1521.

SHCHUKIN, V. K. 1967 Generalisations of experimental data on heat transmission in tubes with vortex generating strips. *Izv. VUZ, Aviasionnaya Tekh.* **10**, 119–126.

SIDDHARTHA, V. 1971 Boundary layers with swirl. Ph.D. thesis, Imperial College, London.

SMITHBERG, G. & LANDIS, F. 1964 Friction and forced convection heat transfer characteristics in tubes with twisted tape swirl generators. *J. Heat. Transfer, Trans. A.S.M.E.* **86**, 39–49.

TALBOT, L. 1954 Laminar swirling pipe flow. *J. Appl. Mech.* **21**, 1–7.

TOWNSEND, A. A. 1956 *The Structure of Turbulent Shear Flow.* Cambridge University Press.

WOLF, L., LAVAN, Z. & FEJER, A. A. 1969 Measurements of the decay of swirl in turbulent flow. *A.I.A.A. J.* **7**, 971.

YAJNIK, K. S. & SUBBAIAH, M. V. 1971 An experimental investigation of turbulent pipe flow with swirl. *3rd Conf. on Fluid Mech. & Fluid Power Ind. Inst. Tech., Kharagpur.*

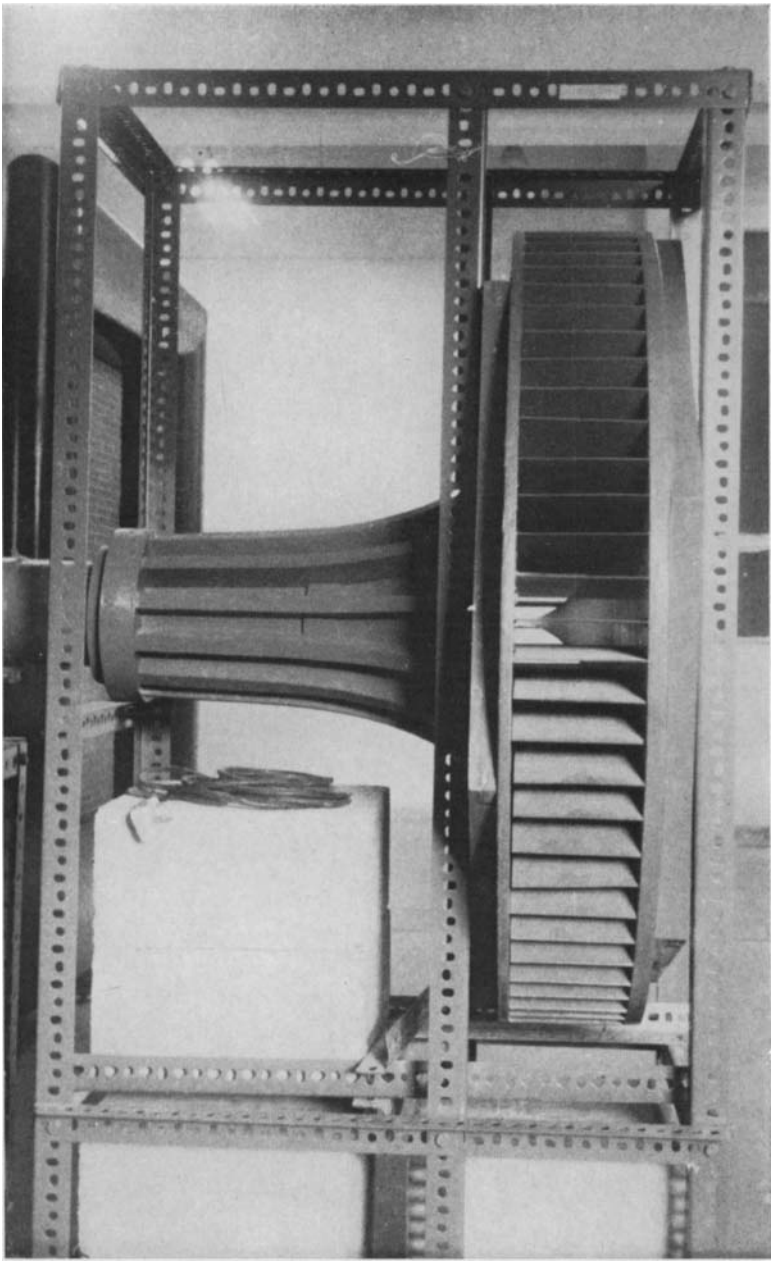

FIGURE 2. Entry section with swirl generating vanes.